Письма в ЭЧАЯ. 2015. Т. 12, № 4(195). С. 957–968

RECONSTRUCTION OF MULTISTRANGE HYPERONS WITH THE MPD DETECTOR AT THE NICA COLLIDER: A MONTE CARLO FEASIBILITY STUDY

M. Ilieva, V. Kolesnikov, D. Suvarieva, V. Vasendina, A. Zinchenko[1]

Joint Institute for Nuclear Research, Dubna

One of the main tasks of the NICA/MPD physics program is a study of strangeness production in nuclear collisions. In this paper the MPD detector performance for measurements of Λ, Ξ^- and Ω^- hyperons and their antiparticles $\bar{\Lambda}$, $\bar{\Xi}^+$ and $\bar{\Omega}^+$ in central Au + Au collisions at NICA energies is presented.

Одной из основных задач физической программы эксперимента MPD на комплексе NICA является изучение рождения странности в ядерных взаимодействиях. В данной работе представлены возможности детектора MPD по измерению гиперонов Λ, Ξ^- и Ω^- и их античастиц $\bar{\Lambda}$, $\bar{\Xi}^+$ и $\bar{\Omega}^+$ в центральных взаимодействиях Au + Au при энергиях NICA.

PACS: 14.20.Jn; 13.75.Ev; 29.40.-n; 29.20.db

INTRODUCTION

The main goal of studying heavy-ion collisions is to explore the properties of nuclear matter under extreme density and temperature conditions. Lattice QCD calculations [1] predict that at the energy density above 1 GeV/fm^3 the nuclear matter undergoes a phase transition to the state of deconfined quark and gluons — Quark–Gluon Plasma (QGP). Such energy densities are released in head-on collisions of heavy ions at energies ($\sqrt{s}$) of several GeV. At present, lots of experimental data on nuclei–nuclei collisions are obtained at high and ultra-high collision energies at SPS, RHIC and LHC [2], while the region of the QCD phase diagram of non-zero baryon densities is mostly unexplored up to now. A new experimental program at the NICA accelerator complex at JINR (Dubna) is aimed to close this gap by performing a comprehensive study of dense nuclear matter in the range of collision energies from $\sqrt{s} = 4A$ to $11A$ GeV. The NICA physics program with heavy ions will address the following topics: study of the properties of the deconfinement phase transition, experimental investigation on medium modification of vector mesons, and search for the QCD critical end point [3].

Production of strange particles is of particular interest because enhanced production of rare strange hadrons ($\bar{\Lambda}, \bar{\Omega}$) in A + A collisions (relative to the yields from elementary *pp* reactions)

[1]E-mail: Alexander.Zinchenko@jinr.ru

was predicted as a signal for the QGP formation [4]. It occurs because the mass of the strange quark ($\sim$ 150 MeV) is comparable to the temperature of the QGP and in the deconfined phase the abundances of parton species should quickly reach their equilibrium values via frequent quark and gluon inelastic scattering processes, thus resulting in a higher yields of strangeness compared to that from a hadron gas (HG). The enhancement of the strangeness was experimentally observed at SPS [5] and RHIC [6], and it is more pronounced for hyperons with larger strangeness content (cascades and omegas). However, in order to prove or rule out the strangeness enhancement as a QGP indicator, one needs to exclude all other conventional mechanisms. For example, it is known for a quite some time that the formation of a dense, long-lived hadronic gas could also produce an increased yield of strange particles through associated production and strangeness exchange reactions [7]. The amount of strangeness enhancement is, however, sensitive to the lifetime of the fireball created in a collision, and in the HG scenario the time interval needed for strange hadrons to reach chemical equilibrium exceeds considerably the lifetime of the fireball [8]. In [9] it was suggested that in dense hadronic systems fast redistribution of strange and light quarks into strange baryon–antibaryon pairs might be achieved by multimesonic fusion type reactions. Recently, it has also become clear that for $p+p$ collisions (used as a reference in strangeness enhancement quantification) canonical suppression effects are important and account (at least, partially) for the overall hyperon enhancement in $A+A$ interactions [10].

At present, a complete theoretical description of the (multi)strangeness production mechanism at collision energies ($\sqrt{s}$) of several GeV has not yet been achieved. In order to better understand the dynamics of hot and dense hadronic matter, the MPD experiment at NICA [11] will provide new precise experimental data on the total yields, rapidity, transverse momentum, and azimuthal angle distributions of (anti)hyperons. The production of baryons and antibaryons with different strangeness content will be compared in central heavy-ion collisions and in proton-induced reactions where no QGP formation is expected.

The goal of this study is to evaluate the performance of the MPD detector for reconstruction of cascade and omega (anti)hyperons.

1. DETECTOR GEOMETRY, EVENT GENERATOR AND DATA SETS

The detailed description of the MPD geometry can be found in [11, 12]. The present analysis is based on the detectors covering the mid-rapidity region ($|\eta| < 1.3$): the main tracker Time Projection Chamber (TPC) and barrel Time-Of-Flight system (TOF), comprising a so-called start version. The overall detector material budget is dominated by the contribution from the TPC inner and outer cages which are multilayer structures made of composite materials like kevlar and tedlar with a high tensile strength and long radiation length. As a result, the total amount of the material does not exceed 10% of the radiation length in the region of interest.

The event samples of central Au + Au collisions (0$-$3.0 fm) for the present study have been produced with the UrQMD generator [13] at $\sqrt{s} = 9A$ GeV. The number of events ranged from 10^4 (for Λ) to $5 \cdot 10^5$ (for $\bar{\Omega}^+$). Particles produced by the event generator have been transported through the detector using the GEANT3 transport package (describing particle decays, secondary interactions, etc.).

2. DETECTOR PERFORMANCE

2.1. Track Reconstruction. The track reconstruction method is based on the Kalman filtering technique (see, e.g., [14]). The number of TPC points per track is required to be greater than 10 to ensure precise momentum and dE/dx measurements. In addition, we have restricted our study to the mid-rapidity region with $|\eta|$ <1.3. The track finding efficiency in TPC for primary and secondary tracks is shown in Fig. 1 as a function of the track transverse momentum. The secondary track sample includes particles produced within 50 cm of the primary vertex in both transverse and longitudinal directions except electrons and positrons from photon conversion, which are not relevant for the current study. The transverse momentum resolution as a function of p_T can be seen in Fig. 1, *b*. These results have been obtained with the assumption on the TPC coordinate resolution of 0.5 and 1.0 mm in transverse and longitudinal directions, respectively. Figure 2, *a* shows the transverse and longitudinal position uncertainties of primary tracks at the point of the closest approach to the main interaction vertex versus track momentum. These detector characteristics are important for secondary vertex reconstruction.

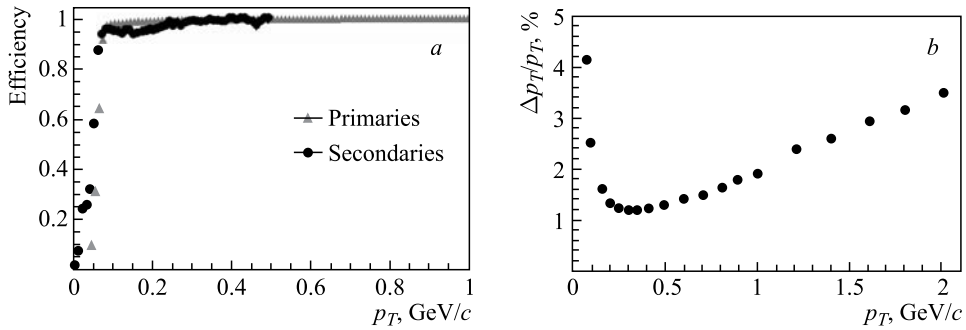

Fig. 1. *a*) Track reconstruction efficiency as a function of track p_T for primary and secondary particles; *b*) relative transverse momentum resolution for primary tracks with $|\eta| < 1.3$ reconstructed in TPC

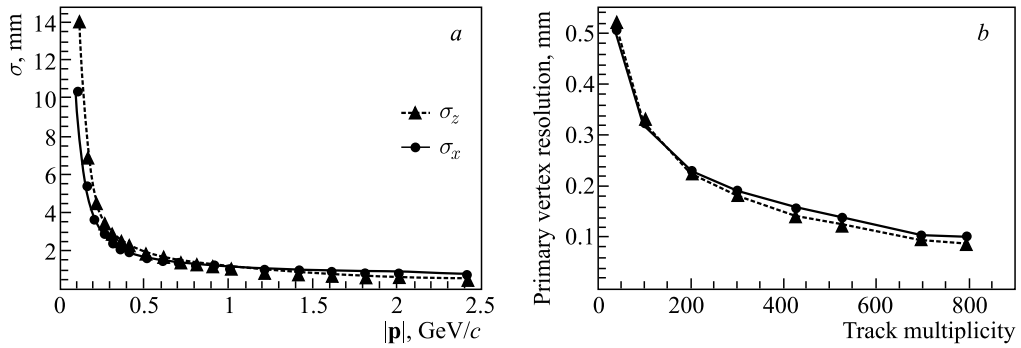

Fig. 2. *a*) Transverse and longitudinal position errors in the point of the closest approach (PCA) to the interaction point for TPC reconstructed primary tracks with $|\eta| < 1.3$ versus particle momentum; *b*) transverse and longitudinal position errors of the reconstructed primary vertex as functions of track multiplicity

Both the primary and secondary vertex reconstruction methods utilized make use of a similar approach based on the Kalman filtering formalism [15]. The primary vertex reconstruction errors as functions of the track multiplicity in the event are shown in Fig. 2, *b*.

For all the tracks reconstructed in the TPC the specific energy loss dE/dx is calculated as a truncated mean of the charges of TPC hits assigned to the tracks. The truncation level of 70% was chosen; i.e., 30% of hits with the highest charges were excluded from the mean value.

Next, the TPC reconstructed tracks are extrapolated to the TOF detector and matched to the TOF hits. For the matched candidates the mass square (M^2) is derived through the relation

$$M^2 = (|\mathbf{p}|/q)^2 \left(\frac{c^2 t^2}{l^2} - 1 \right),$$

where $|\mathbf{p}|/q$ is the ratio of the track momentum $|\mathbf{p}|$ to the particle's charge q (*magnetic rigidity*); t is the time of flight from TOF; l is the path length from the collision vertex to the TOF hit; and c is the speed of light.

2.2. Particle Identification. Particle identification (PID) in the MPD experiment will be achieved by combining specific energy loss (dE/dx) and time-of-flight measurements. The basic detector parameters, namely, dE/dx and TOF resolutions of $\sigma_{dE/dx} \approx 6\%$ and $\sigma_{\mathrm{TOF}} \approx 100$ ps will provide a high degree of selectivity for hadrons at momenta below 2 GeV/c (see Fig. 3). An identified hadron candidate is assumed to lie within the boundaries of the PID ellipse (3σ around the nominal position for a given particle species). In addition, the probability for a given particle to belong to each of the species can be calculated knowing the widths of the corresponding distributions (along the dE/dx and M^2 axes) and the difference from the predicted position for the species. It was found that by requiring this probability to be greater than 0.75 one can get distributions for the PID efficiency and contamination of wrongly identified hadrons shown in Fig. 4. The PID efficiency is defined as a ratio of correctly tagged to the total number of reconstructed particles matched with TOF, where the overall (integrated over p_T and $|\eta| < 1.3$) TPC–TOF matching efficiency is about 95%. The contamination is determined as the number of incorrectly tagged particles divided by the number of correctly tagged particles. As can be seen from Fig. 4, the PID efficiency for protons is close to 1.0, while due to a partial overlap of the distributions for pions and kaons at momenta above $|\mathbf{p}| = 0.7$ GeV/c, the PID efficiency for charged kaons drops down to ≈ 0.6 at $|\mathbf{p}| = 2.5$ GeV/c. We also observe a significant contamination of mis-identified particles in the antiproton sample at momenta below 0.5 GeV/c. It was found that the source of this background is the secondary protons produced in the outer vessels of the TOF and TPC detectors and moving inward (that is in the opposite to the "normal"

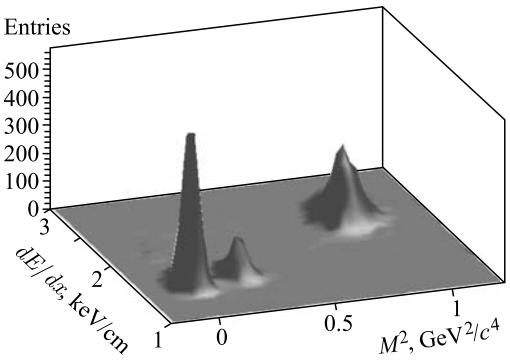

Fig. 3. A typical distribution of the specific energy loss dE/dx versus mass squared for π^+, K^+, and protons (from left to right) at $|\mathbf{p}| = 1$ GeV/c

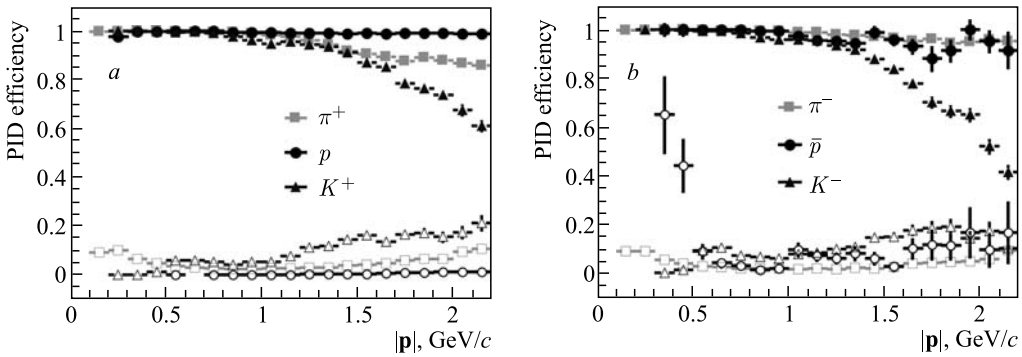

Fig. 4. PID efficiency (filled symbols) and contamination of wrongly identified particles (empty symbols) as a function of the total momentum for positively charged hadrons (*a*) and negatively charged particles (*b*)

(outward) flow of the particles born in the primary interaction). Since the track reconstruction procedure treats them as "normal" tracks, they are identified as antiprotons due to wrongly assigned charge. These protons, however, are produced almost isotropically and in most cases being extrapolated back to the main vertex pass far away from it. Thus, by applying a cut on the distance of the closest approach between the track and the main vertex, we can suppress this background lowering it to a few percent level.

3. ANALYSIS PROCEDURE

3.1. Hyperon Reconstruction and MpdParticle Object. We reconstruct (multi)strange hyperons by combining charged tracks reconstructed in the TPC, first to select a V_0-candidate (a characteristic topology of two oppositely charged daughter tracks) and then to match it with one of the secondary pion or kaon candidate. In Fig. 5 is drawn a pictorial representation of the decay topology for Λ and Ω hyperons in the bending plane of the magnetic field. In order to

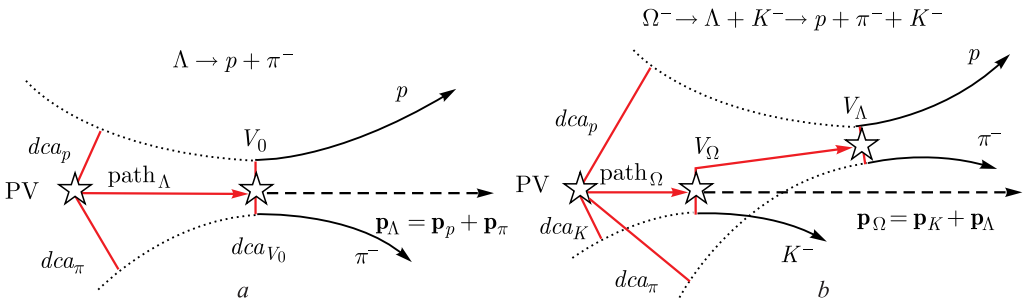

Fig. 5. *a*) Event topology of two-particle decays of a neutral particle (e.g., $\Lambda \to p + \pi^-$); *b*) event topology of cascade-type decays (e.g., $\Omega^- \to \Lambda + K^- \to p + \pi^- + K^-$) (transverse view). Here dca_p, dca_π and dca_K are the distances of the closest approach of the decay tracks to the primary vertex PV, dca_{V_0} is the distance between daughter tracks in the decay vertex V_0, path is the decay length, $\mathbf{p}_p$, $\mathbf{p}_\pi$, $\mathbf{p}_K$, $\mathbf{p}_\Lambda$ and $\mathbf{p}_\Omega$ are momenta of particles

reject wrong track combinations, we applied several selection criteria: the geometric variables used are shown in Fig. 5. To ensure that the charged tracks are secondary ones, special cuts are applied on the minimum value of the impact parameters to the primary vertex ($dca_{K,p,\pi}$). Next, the track combination is rejected if the distance of the closest approach (dca_{V_0}) in space between the two oppositely charged tracks or the pointing angle, defined as the angle between the mother particle momentum and the direction vector from the primary to the secondary vertex, are larger than given values. To further suppress mostly primary track combinations, it is also required that the secondary vertex position should be at a certain distance from the primary one (path). Finally, the invariant mass is calculated under the proper particle hypothesis, i.e., a proton and a pion for the case of V_0 or Λ and a kaon for Ω hyperon.

The exact values of selection cuts (Table 1) were found by performing a multidimensional scan over the whole set of selection criteria with a requirement to maximize the invariant mass peak significance, defined as $S/\sqrt{S+B}$, where S and B are total numbers of signal (described by the Gaussian) and background (polynomial function) combinations inside $\pm 2\sigma$ interval around the peak position. While different physics analyses might prefer different selection quality criteria, the significance looks convenient to quantitatively evaluate effect of different factors on the reconstruction quality. The corresponding scan procedure was realized as follows: during the particle combinations the parameters which have been chosen to serve as selection criteria (see above) were recorded along with the invariant mass value. Later, multiple loops over those variables were performed in some steps and their values were used as low or high thresholds, yielding the invariant mass peak significance for each set of selection cut values. Then, the maximum value was taken along with the corresponding set of selection parameters. It was found that both the DCA and two-track separation cuts are more efficient if applied in χ^2-space, i.e., if normalized to their respective errors. So, these values were calculated along with the parameters of decay vertices and daughter and mother particles (including neutral ones).

Since the decay chain usually happens quite close to the beam line where, in the current detector configuration, there are no detector measurements available, for reasons of efficiency the task of secondary vertex reconstruction was decoupled from the track reconstruction

Table 1. **Selection cuts corresponding to the maximum significance of the invariant mass peak: χ^2_m and χ^2_b are normalized to the number of degrees of freedom χ^2/NDF of decay mesons (π or K) and baryons ((anti)protons or (anti)lambdas) with respect to the primary vertex, χ^2_V is the secondary vertex fit quality, path is the decay length and angle is the pointing angle (see the text). Selected particle combinations should satisfy the following conditions: $\chi^2_m > c_1$ && $\chi^2_b > c_2$ && $\chi^2_V < c_3$ && path $> c_4$ && angle $< c_5$, where c_i are the cut values**

Particle	Selection cuts				
	χ^2_m	χ^2_b	χ^2_V	Path, cm	Angle
Λ	3.8	3.0	2.8	2.6	0.09
$\bar{\Lambda}$	3.5	2.0	2.3	2.7	0.11
Ξ^-	9.5	12.5	2.5	3.3	0.09
$\bar{\Xi}^+$	6.5	6.5	3.8	1.7	0.10
Ω^-	4.7	7.6	2.8	1.6	0.08
$\bar{\Omega}^+$	2.9	3.5	2.4	1.4	0.11

one. Within the object-oriented approach realized in the MpdRoot software framework [16] it required introducing a separate analysis-oriented object MpdParticle with its respective methods which can be created from reconstructed tracks or other MpdParticles (both charged and neutral) and fulfills the above-mentioned tasks. Following the synergy paradigm, the concept of such an analysis object was adopted from a so-called KF Particle of the CBM experiment [17]. However, the implementation had to be different due to difference in the detector configuration (collider against fixed target) and was based on the formalism described in [15].

3.2. Event Mixing. Monte Carlo study of rare probes in heavy-ion collisions (especially in the central ones) is a very computer-intensive task in terms of CPU power and disk storage consumption due to high multiplicity of produced particles. That is why different approaches were proposed aimed at making the simulation procedures more "economical". In case of hyperon reconstruction by calculating the invariant mass distribution of particle combinations, the main task of such techniques is to reproduce the combinatorial background, which can be realized within the so-called event mixing schemes.

We also tried to test such approaches for simulation of Ω^- and $\bar{\Omega}^+$ hyperons where both the "normal" event samples and mixed ones were used in order to check validity of event mixing techniques. We used the following, embedding-like, approach: an event sample was artificially enriched such that in each event was the studied probe (Ω^- or $\bar{\Omega}^+$). The phase-

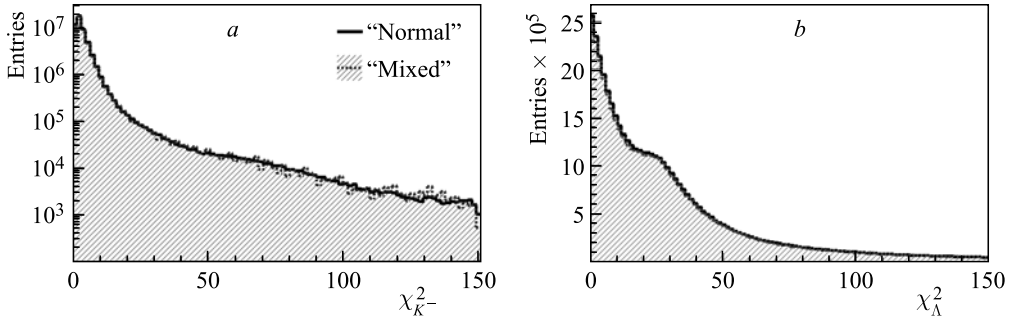

Fig. 6. Distribution of χ^2 to the primary vertex of K^- (*a*) and Λ (*b*) candidates

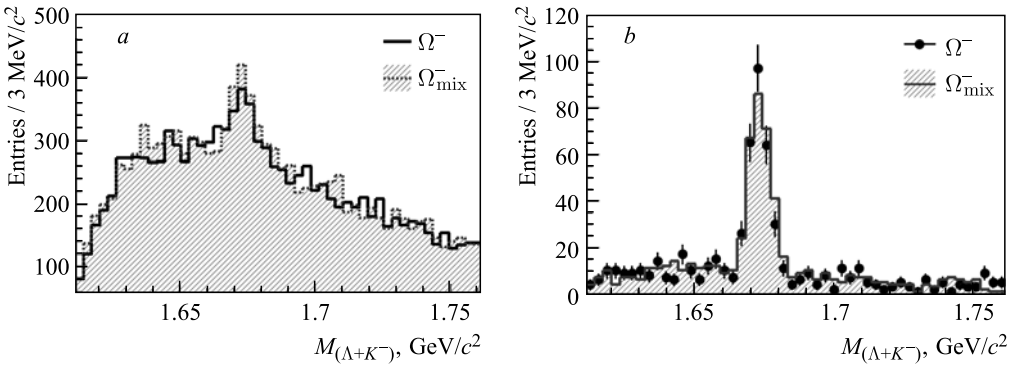

Fig. 7. Reconstructed invariant mass of K^- and Λ candidates with moderately tight (*a*) and final (*b*) selection cuts

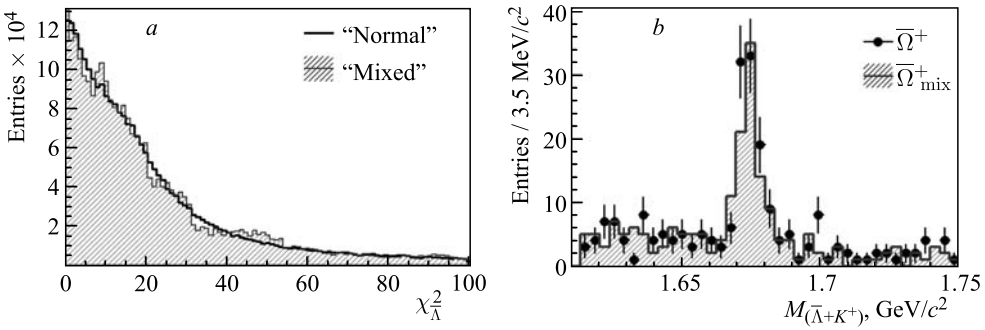

Fig. 8. Distribution of χ^2 to the primary vertex of $\bar{\Lambda}$ candidates (*a*) and reconstructed invariant mass of K^+ and $\bar{\Lambda}$ candidates after final selection cuts (*b*)

space distribution of the embedded particles was the same as in the UrQMD model. In order to construct the event-mixing distribution, we combine each reconstructed Λ ($\bar{\Lambda}$)-hyperon candidate from an event with all kaon candidates from several events, where the number of events to mix is defined by the Ω^- ($\bar{\Omega}^+$) production rate in "normal" events ($1\Omega^-$ per $\sim$13 events or $1\bar{\Omega}^+$ per $\sim$100 events in our cases).

To validate the procedure, distributions of event variables, relevant for Ω^- candidate selection, were produced for both the "normal" and "mixed" event samples (Figs. 6 and 7). One can see that the "mixed" distributions very closely reproduce the "normal" ones.

When trying to apply the same approach to the $\bar{\Omega}^+$ case, we found that the background description significantly deteriorated due to lack of $\bar{\Lambda}$ candidates in the mixed sample, resulting in much larger fluctuations as compared to the "normal" case. To deal with that, the procedure has been changed in the following way: at the beginning of the processing $\bar{\Lambda}$ candidates were recorded for the whole event sample and later used for the mixing by randomly selecting the event number. As a result, the agreement between "mixed" and "normal" distributions has improved, still showing somewhat excessive fluctuations in some distributions (see Fig. 8, *a*), which potentially could affect the final selection result (did not in our case — Fig. 8, *b*). Nevertheless, this result demonstrates the necessity to produce statistically significant samples of "mixture components" and properly use them in the event mixing procedure.

4. RESULTS AND DISCUSSION

4.1. Reconstruction of Λ ($\bar{\Lambda}$) Hyperons. The results (Fig. 9 and Table 2) have been obtained for 10^4 (for Λ) and $4 \cdot 10^4$ (for $\bar{\Lambda}$) central Au + Au events (0–3.0 fm) at $\sqrt{s} = 9A$ GeV. This corresponds to about 30 s and 2 min of data taking time, respectively.

Table 2 shows the effect of the detector acceptance (i.e., η-coverage and low-p_T cut for Λ ($\bar{\Lambda}$) decay products) on hyperon detection efficiency where the efficiency is defined with respect to the total number of hyperons. Lines 2–5 demonstrate the effect of the p_T cut on the efficiency, where p_T is the true transverse momentum of the decay pion and proton. Line 6 shows the reconstruction efficiency, i.e., considering the decay pions and protons reconstructed in the detector without any explicit p_T cut (and without PID efficiency). The last line includes all the relevant factors, i.e., reconstruction and PID efficiencies as well as

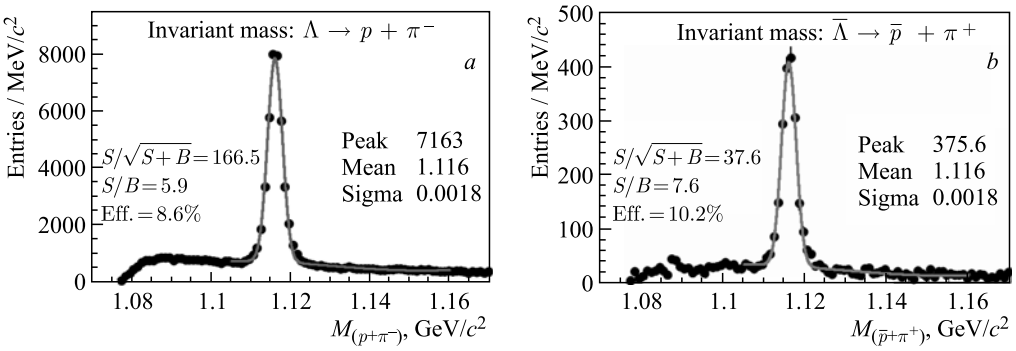

Fig. 9. Reconstructed invariant mass of proton and π^- (*a*) and $\bar{p}$ and π^+ (*b*)

Table 2. **Factors affecting Λ ($\bar{\Lambda}$) reconstruction efficiency**

Factor	Efficiency, %	
	Λ	$\bar{\Lambda}$
Branching ratio: $\Lambda \to p + \pi^-$ ($\bar{\Lambda} \to \bar{p} + \pi^+$)	63.4	63.5
p and π^- ($\bar{p}$ and π^+) at $\lvert\eta\rvert < 1.3$	29.9	35.1
p and π^- ($\bar{p}$ and π^+) at $\lvert\eta\rvert < 1.3$ and $p_T > 0.05$ GeV/c	28.3	32.9
p and π^- ($\bar{p}$ and π^+) at $\lvert\eta\rvert < 1.3$ and $p_T > 0.1$ GeV/c	22.0	26.0
p and π^- ($\bar{p}$ and π^+) at $\lvert\eta\rvert < 1.3$ and $p_T > 0.2$ GeV/c	8.6	10.3
Reconstructed p and π^- ($\bar{p}$ and π^+) at $\lvert\eta\rvert < 1.3$	22.7	26.5
Maximum siginificance	8.6	10.3

selection efficiency. One can see that the detector provides efficient reconstruction of hyperons with p_T of decay tracks above 0.1 GeV/c in good agreement with Fig. 1. It is also clear that a higher p_T threshold (e.g., 0.2 GeV/c) would significantly reduce the detector efficiency. The efficiency drop due to selection cuts comes from the necessity to suppress the combinatorial background in order to obtain a clean invariant mass peak.

One can also see that, in spite of much lower production rate for antilambdas relative to the one for Λ ($\bar{\Lambda}/\Lambda \approx 10^{-2}$ in central Au + Au at $\sqrt{s} = 9A$ GeV), the obtained results for both the selection and total efficiencies are better than those for Λ. This is due to a higher fraction of antiprotons from weak decays in the total $\bar{p}$ sample as compared to the proton case.

4.2. Reconstruction of Multistrange Hyperons. The results for Ξ^- and $\bar{\Xi}^+$ hyperons (Table 3 and Fig. 10) have been obtained for $4 \cdot 10^4$ (for Ξ^-) and $3 \cdot 10^5$ (for $\bar{\Xi}^+$) central Au + Au events at $\sqrt{s} = 9A$ GeV. This corresponds to about 2 and 17 min of running time at the NICA collision rate of 6 kHz, respectively. Here, Λ ($\bar{\Lambda}$) candidates in the invariant mass interval $\pm 3\sigma$ around the peak position were combined with negative (positive) pions to form Ξ^- ($\bar{\Xi}^+$) candidates. It should be noted here that the pointing angle cut (see Table 1) for Λ ($\bar{\Lambda}$) candidates has been relaxed to ~ 0.3 in order not to reject decay products of the cascades.

The results for Ω^- and $\bar{\Omega}^+$ (Fig. 11 and Table 3) have been obtained for $3 \cdot 10^5$ and $5 \cdot 10^5$ events for Ω^- and $\bar{\Omega}^+$ hyperons, respectively, corresponding to about 17 and 28 min of data taking time at NICA. Here the necessity of suppressing a larger combinatorial background

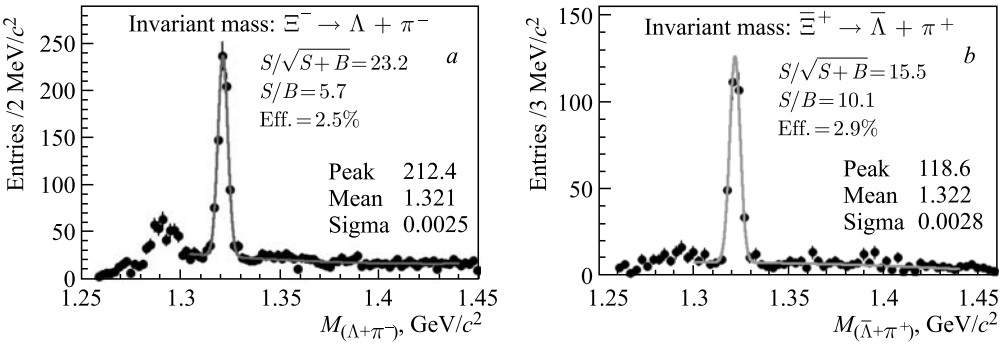

Fig. 10. Reconstructed invariant mass of Λ candidate and π^- (*a*) and $\bar{\Lambda}$ candidate and π^+ (*b*)

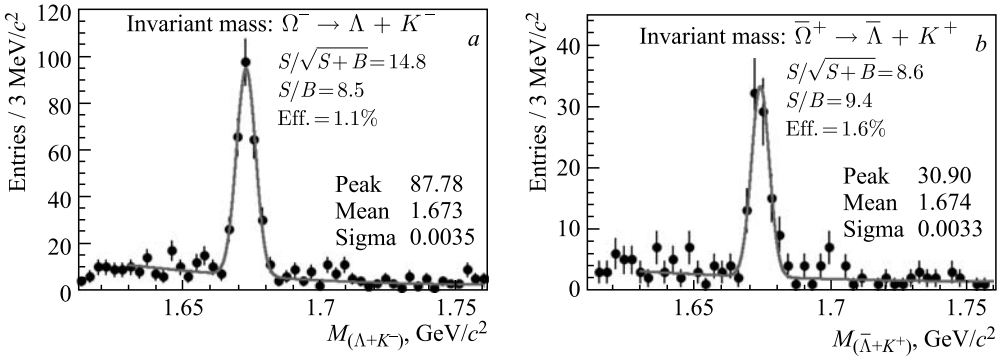

Fig. 11. Reconstructed invariant mass of Λ candidate and K^- (*a*) and $\bar{\Lambda}$ candidate and K^+ (*b*)

Table 3. **Factors affecting $\Xi^\mp$ and $\Omega^\mp$ reconstruction efficiency. The notations are: 0 — $\Lambda(\bar{\Lambda})$; 1 — $p(\bar{p})$; 2, 3 — $\pi^-(\pi^+)$; 4 — $K^-(K^+)$**

Factor	Efficiency, %			
	Ξ^-	$\bar{\Xi}^+$	Ω^-	$\bar{\Omega}^+$
Branching ratio: $\Xi^\mp \to 0+3$, $\Omega^\mp \to 0+4$				
$\hookrightarrow 1+2$ $\hookrightarrow 1+2$	63.6	63.1	42.8	42.2
1, 2 and 3(4) at $\lvert\eta\rvert < 1.3$	27.2	28.6	18.4	17.7
1, 2 and 3(4) at $\lvert\eta\rvert < 1.3$ and $p_T > 0.05$ GeV/c	24.6	25.7	17.2	16.6
1, 2 and 3(4) at $\lvert\eta\rvert < 1.3$ and $p_T > 0.1$ GeV/c	15.0	16.0	12.2	11.7
1, 2 and 3(4) at $\lvert\eta\rvert < 1.3$ and $p_T > 0.2$ GeV/c	2.9	3.0	3.6	3.2
Reconstructed 1, 2 and 3(4) at $\lvert\eta\rvert < 1.3$	16.3	16.8	10.0	9.3
Maximum significance	2.5	2.9	1.1	1.6

and a requirement to have a sufficient significance of the signal resulted in stronger cuts and lower efficiencies. Also, as in the case of lighter hyperons, we observed a large drop in the overall reconstruction efficiency when the low-p_t cut-off of decay products was increased from 0.1 to 0.2 GeV/c. Therefore, the MPD detector's ability of reconstructing very low

momentum particles (at least, down to $p_T = 0.1$ GeV/c) is of crucial importance for measurements of multistrange hyperons.

5. SUMMARY

The capability of the MPD detector to reconstruct Λ ($\bar{\Lambda}$), Ξ^- ($\bar{\Xi}^+$) and Ω^- ($\bar{\Omega}^+$) hyperons in central Au + Au collisions at $\sqrt{s} = 9A$ GeV was investigated. The UrQMD event generator was used as the input for the Monte Carlo simulation study of the detector set-up comprising the Time-Projecting Chamber (TPC) and barrel Time-Of-Flight (TOF) system. Particle identification was achieved by combining the energy loss (from TPC) and time-of-flight (from TOF) measurements. In order to facilitate the physics analysis for MPD a special software object MpdParticle was designed and implemented within the MpdRoot framework. In addition, some event-mixing techniques intended to enhance the ability to do feasibility studies of rare probes were developed and validated. Reliable extraction of all the hyperon species under study was demonstrated to be possible. A special procedure aimed at the maximization of the significance of the reconstructed invariant mass peak was applied, resulting in the observed signal-to-background ratio $S/B \gtrsim 6$. The invariant mass resolution of ≈ 3 MeV/c^2 was achieved. Based on the results of this study and model predictions, we have estimated the expected yields of particle species of interest for 10 weeks of data taking (see Table 4).

Table 4. **Expected particle yields in central Au + Au collisions for 10 weeks of running time**

Particle	Λ	$\bar{\Lambda}$	Ξ^-	$\bar{\Xi}^+$	Ω^-	$\bar{\Omega}^+$
Expected yield	$5.8 \cdot 10^9$	$7.3 \cdot 10^7$	$2.9 \cdot 10^7$	$1.6 \cdot 10^6$	$1.4 \cdot 10^6$	$2.9 \cdot 10^5$

REFERENCES

1. *Fodor Z., Katz S. D.* Critical Point of QCD at Finite T and μ, Lattice Results for Physical Quark Masses // JHEP. 2004. V. 0404. P. 050.
2. For a review, see materials from the recent Quark Matter Conference. http://qm2014.gsi.de/.
3. Searching for a QCD Mixed Phase at the Nuclotron-Based Ion Collider Facitility (NICA White Paper). https://indico.cern.ch/event/275003/contribution/1/material/paper/0.pdf.
4. *Rafelski J., Muller B.* Strangeness Production in the Quark–Gluon Plasma // Phys. Rev. Lett. 1982. V. 48. P. 1066.
5. *Antinori F. (NA57 Collab.).* Strangeness Enhancements at Central Rapidity in $40A$ GeV/c Pb–Pb Collisions // J. Phys. G. 2010. V. 37. P. 045105.
6. *Abelev B. I. (STAR Collab.).* Enhanced Strange Baryon Production in Au + Au Collisions Compared to $p + p$ at $\sqrt{s_{NN}} = 200$ GeV // Phys. Rev. C. 2008. V. 77. P. 044908.
7. *Matsui T., Svettisky B., McLerran L. D.* Strangeness Production in Ultrarelativistic Heavy Ion Collisions: 2. Evolution of Flavor Composition in Scaling Hydrodynamics // Phys. Rev. D. 1986. V. 34. P. 2047.
8. *Cassing W., Bratkovskaya E. L., Juchem S.* Excitation Functions of Hadronic Observables from SIS to RHIC Energies // Nucl. Phys. A. 2000. V. 674. P. 249.

9. *Greiner C., Leupold S.* Anti-Hyperon Production in Relativistic Heavy Ion Collision // J. Phys. G. 2001. V. 27. P. L95.
10. *Tounsi A., Redlich K.* Strangeness Enhancement and Canonical Suppression. arXiv:hep-ph/0111159.
11. *Abraamyan K. U. (MPD Collab.).* The MPD Detector at the NICA Heavy-Ion Collider at JINR // Nucl. Instr. Meth. A. 2011. V. 628. P. 99.
12. http://nica.jinr.ru/files/CDR_MPD/MPD_CDR_en.pdf
13. http://urqmd.org/
14. *Fruhwirth R.* Application of Kalman Filtering to Track and Vertex Fitting // Nucl. Instr. Meth. A. 1987. V. 262. P. 444.
15. *Luchsinger R., Grab Ch.* Vertex Reconstruction by Means of the Method of Kalman Filter // Comp. Phys. Commun. 1993. V. 76. P. 263.
16. http://mpd.jinr.ru/
17. *Gorbunov S., Kisel I.* Reconstruction of Decayed Particles Based on the Kalman Filter. CBM-SOFT-note-2007-003. 2007.

Received on November 27, 2014.